# Equivalent Circuit Model for Large-Area Photodiodes for VLC Systems

Amany Kassem and Izzat Darwazeh
*Department of Electronic and Electrical Engineering*
*University College London*
London, United Kingdom
amany.kassem.15@ucl.ac.uk, izzat.darwazeh@ucl.ac.uk

***Abstract*—An equivalent circuit model for large-area PIN photodiodes used in visible light communication (VLC) applications is described. The modelling aims to gain insight into the effect of the photodiode intrinsic elements on the bandwidth of VLC receivers. The model parameters are extracted based on impedance measurements of two commercially available large-area PIN photodiodes. The extracted model parameters identify the photodiode series resistance as a major contributor to the bandwidth limitation of VLC receivers, especially when employing low input impedance transimpedance amplifiers (TIAs). However, such resistance is commonly ignored by most circuit designers, since it is assumed to have a negligible effect on the TIA performance. To demonstrate the accuracy of the photodiode equivalent circuit model, a design example of a low input impedance regulated cascode (RGC) TIA is described. The TIA is constructed using discrete components and a printed circuit board (PCB). The designed RGC TIA is measured using the proposed photodiode equivalent model versus a simplified model. In addition, a VLC link is constructed to measure the optoelectrical response of the large-area photodiode with the RGC TIA. The RGC frequency response measurements obtained from the full and simplified photodiode equivalent model are contrasted to the optoelectrical response, which verified that, unlike the simplified photodiode model, the proposed photodiode equivalent model can accurately predict the bandwidth performance of the VLC receiver.**

***Index Terms*—photodiodes, optical receivers, visible light communications**

## I. Introduction

Knowledge of the photodiode equivalent model is essential for designing optimised transimpedance amplifiers (TIAs) in optical receivers. Such a requirement is particularly critical for visible light communication (VLC) systems, which introduces some idiosyncrasies that impose additional design constraints on the TIA. Firstly, the nature of the free-space channel, whose loss is inversely proportional to the square of the transmission distance. Secondly, most photodiodes operating in the visible range are silicon, with relatively poor responsivity in the visible range, limiting the converted photocurrent. Therefore, to boost signal detection in VLC, a combination of a large-area photodiode and high gain TIA is desirable to detect the transmitted signal correctly [1, 2].

Large-area photodiodes are associated with high junction capacitance ($C_{pd}$), which limits the receiver bandwidth, particularly for TIAs with a 50 Ω or high input impedance. Using low input impedance TIAs configuration is advantageous in tolerating high $C_{pd}$. This is because the dominant time constant, which determines the receiver bandwidth, is a product of $C_{pd}$ and the TIA input resistance. Hence, a TIA with low input resistance reduces the time constant and significantly increases the receiver bandwidth. Circuits with low input resistance, such as the common base (CB) [3, 4] and the regulated cascode (RGC) TIAs [5], originally proposed for earlier generations of optical fibre communication systems, are more recently found to be highly attractive for use in VLC systems [6–9]. For example, our recent work in [6] reports a specially designed modified RGC TIA for large-area photodiodes, achieving a bandwidth of 200 MHz at 2 kΩ with an equivalent $C_{pd}$ of 300 pF. Such remarkable bandwidth performance at an exceptionally high $C_{pd}$ is a virtue of the ultra-low input impedance of the RGC TIA. This advantageously improves the utility of large-area photodiodes, therefore allowing for higher detected powers and better signal to noise ratio (SNR), which is a fundamental requirement to enable high data rate long-span VLC links.

Despite the appreciable efforts to report specially designed TIAs for VLC applications in [1, 6, 8, 10]. Nevertheless, such designs are based on a simplified photodiode equivalent circuit model, which models the photodiode behaviour simply as a current source in parallel with a shunt capacitance $C_{pd}$, discarding any potentially bandwidth-limiting effects of other intrinsic elements of the photodiode or extrinsic parasitic factors [6, 8, 10]. For example, the photodiode presents a series resistance, which is often in the range of a few ohms; alas, it became a convention for circuit designers to ignore it, since it is assumed that such resistance has a negligible effect on the TIA performance. Nevertheless, such resistance adds to the TIA input resistance and, in turn, inflicts an additional bandwidth-limiting factor for VLC receivers. This resistance is attributed to the photodiode ohmic contact and other characteristics of the material; techniques to reduce the photodiode series resistance based on a modified internal structure of the photodiode are proposed in [11].

This work investigates the modelling and equivalent parameter extraction of large-area photodiodes for VLC receivers. The photodiode modelling aims to study the effect of the intrinsic elements of the photodiode on its performance when loaded with low input impedance TIAs. One-port reflection measurement, based on the return loss ($S_{11}$), is

This work was supported in part by Engineering and Physical Sciences Research Council (EPSRC) MARVEL under Grant EP/P006280/1

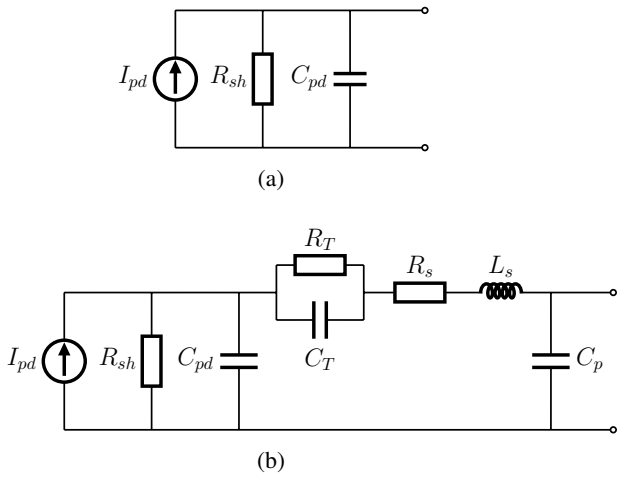


Fig. 1: Photodiode equivalent circuit model (a) Simplified RC circuit model (b) Full equivalent circuit model

a commonly used approach to characterise the equivalent circuit model of optoelectronic devices such as lasers [12], LEDs [13–15] and photodiodes [16, 17]. In [16], this was adopted to report a high-frequency model and parameter extraction of three small area InGaAs photodiodes for the application of 40 Gb/s optical receivers. However, there is limited modelling on large-area photodiodes akin to what is used in VLC systems. This work identifies a suitable equivalent model for large-area photodiodes. The model accuracy is validated through parameter extraction of two large-area commercially available PIN photodiodes. The parameter extraction established the presence of a photodiode series resistance that imposes an additional bandwidth-limiting factor on VLC receivers. Therefore, when designing the TIA circuit, care must be taken, especially for low input impedance TIAs. The bandwidth-limiting effect of the photodiode series resistance is demonstrated using a design example of a low input impedance RGC TIA. The TIA is constructed using discrete components on a PCB. The TIA performance is measured based on passive components to emulate the simplified and full photodiode equivalent model. Then, a VLC link is constructed to measure the optoelectrical response of the photodiode with the TIA. Measurements showed that, unlike the simplified equivalent model, the full equivalent model provides much better predictions of the optoelectrical response of the photodiode and the RGC.

## II. Large-Area Photodiode Passive Equivalent Circuit Model

The photodiodes used in VLC are often PIN diodes, which are devices with an intrinsic layer sandwiched between the p-type and n-type layers. Such devices have a depletion region of width $W_D$, which is a function of the photodiode bias voltage $V_B$. Applying negative voltage (reverse bias), increases $W_D$ and therefore reduces the associated junction capacitance $C_{pd}$. The photodiode will also have a shunt bulk resistance $R_{sh}$ given by the slope of its current-voltage curve as defined by the Shockley equation given by

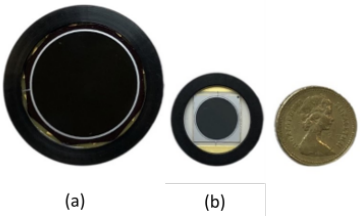


Fig. 2: Photodiodes under-test (a) PIN25-D (600 mm$^2$) (b) PIN10-D (100 mm$^2$)

$I_s exp(qV_B/KT)$, where $I_s$ is the reverse saturation current, $q$ is the electron charge, $K$ is Boltzman constant, and $T$ is the temperature in Kelvin. Hence, such elements, $C_{pd}$ and $R_{sh}$ in parallel with a current source $I_{pd}$, are what forms the most basic photodiode equivalent model shown in Fig. 1a. Typically, $R_{sh}$ is in the order of several MΩ and, as such, behaves like an open circuit. Hence, within the circuit design community, the photodiode model is often simplified to $C_{pd}$ only, with such a model, a diode loaded by a TIA results in a bandwidth determined by an RC time constant, simply given by:

$$f_{3dB} = \frac{1}{2\pi R_a C_{pd}} \tag{1}$$

where $R_a$ is the input resistance of the TIA, commonly designed to be 50 Ω.

Fig. 1b shows the full photodiode equivalent circuit model, which accounts for the photodiode series resistance $R_s$, the feed-line inductance $L_p$ and the pad capacitance $C_p$. In addition to, an RC combination $R_T$ and $C_T$, which were essential to fit the model to the s-parameters of the photodiode adequately and are likely attributed to contacts that are not fully ohmic and display some Schottky behaviour. The sum of resistances $R_s + R_T$ come in series to the TIA input resistance, such that the receiver's bandwidth can be approximated by:

$$f_{3dB} \approx \frac{1}{2\pi(R_s + R_T + R_a)C_{pd}} \tag{2}$$

Clearly, $R_s + R_T$ impose an additional bandwidth-limiting factor on the receiver's bandwidth. $R_s$ is widely associated with the ohmic contacts of the photodiode only. However, in [18], $R_s$ is the sum of the ohmic contact resistance $R_c$, and the resistance of the undepleted region as expressed by:

$$R_s = \frac{(W_s - W_D)\rho}{A} + R_c \tag{3}$$

where $W_s$ and $\rho$ are the thickness and resistivity of the substrate, respectively, and $A$ is the diffused area of the junction. Taking the substrate parameters and area as constant, clearly, $R_s$ is determined by $W_D$, which itself is a function of $V_B$. This suggests that such resistance is not strictly constant but a function of the bias condition. Moreover, interestingly, such resistance is inversely proportional to the photodiode area. Hence, this implies that photodiodes with larger areas will have smaller $R_s$.

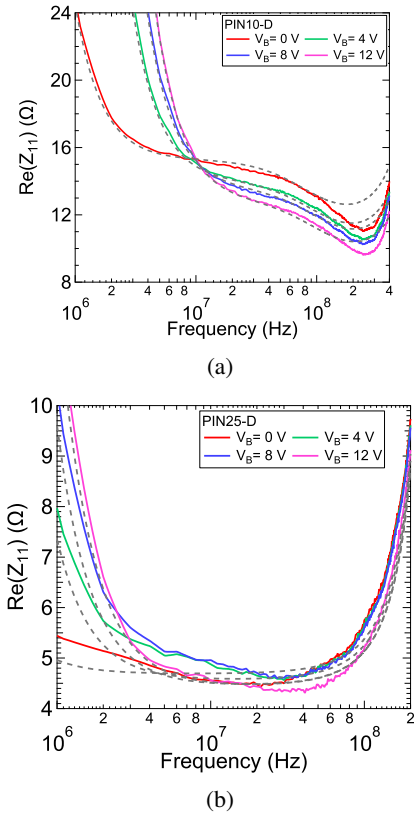


Fig. 3: Measured (solid) and fitted photodiode equivalent circuit model (dashed) Re($Z_{11}$) responses at different $V_B$ (a) PIN10-D (100 mm$^2$) (b) PIN25-D (600 mm$^2$)

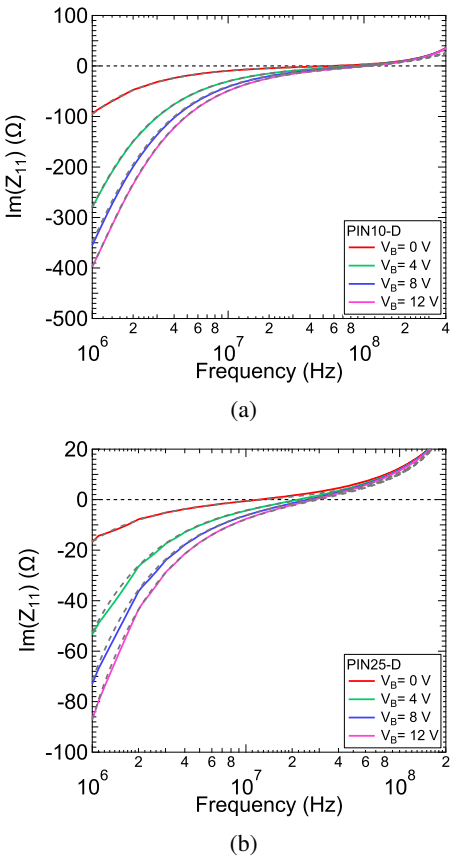


Fig. 4: Measured (solid) and fitted photodiode equivalent circuit model (dashed) Im($Z_{11}$) responses at different $V_B$ (a) PIN10-D (100 mm$^2$) (b) PIN25-D (600 mm$^2$)

## III. Parameter Extraction

This section describes the parameter extraction of two commercially available silicon PIN photodiodes of different areas shown in Fig. 2. The photodiodes are manufactured by OSI Optoelectronics: PIN10-D and PIN25-D of areas 100 mm$^2$ and 600 mm$^2$, respectively. Each photodiode is reverse biased by grounding the anode and applying $V_B$ to the cathode through a bias resistor $R_b$. The cathode is AC-coupled to port 1 of the vector network analyser (VNA) to measure the input reflection coefficient $S_{11}$ of each photodiode at different $V_B$.

The $S_{11}$ is then converted to the corresponding impedance response $Z_{11}$ to obtain the real and imaginary impedance parts, Re($Z_{11}$) and Im($Z_{11}$), equivalent to the resistance and the reactance responses of the photodiode [19]. The parameter extraction is conducted by curve fitting the full photodiode passive equivalent circuit model shown in Fig. 1b to the measured Re($Z_{11}$) and Im($Z_{11}$) responses. The model fitting is limited to 400 MHz for the PIN10-D (100 mm$^2$) and 200 MHz for the PIN25-D (600 mm$^2$). This was chosen according to the operational frequency, which, as demonstrated in Section. IV-B is limited to 40 MHz. Moreover, the model curves are shown starting from 1 MHz; this is to omit the effect of $R_b$, which is most prominent at low frequencies.

### A. Impedance Measurements

Figs. 3 and 4 show the Re($Z_{11}$) and Im($Z_{11}$) of the two photodiodes at different $V_B$, respectively, where clearly the equivalent model agrees well with the measurements. From Fig. 3, Re($Z_{11}$) initially shows a decaying profile, until it reaches a resistive floor, before it shows a rise at higher frequencies attributed to $C_p$. This rise occurs at significantly high frequencies well above the photodiode operational frequency. Nevertheless, an estimation of $C_p$ was included for completeness, which is estimated to be 2 pF for the PIN10-D and 12 pF for the PIN25-D.

More importantly, the resistive floor corresponds to $R_s + R_T$, where the frequency-dependent behaviour is attributed to $C_T$. The resistive floor level strongly depends on the photodiode area, and to a lesser extent, on $V_B$, where increasing $V_B$ results in only a slight reduction in the resistive floor level for each of the photodiodes. In contrast, the resistive floor level is significantly reduced for the photodiode with a larger area. These variations in the resistive floor level are assumed to be due to $R_s$ rather than $R_T$. Since according to (3), the value of $R_s$ is a function of both the photodiode area and $V_B$. Whereas, $R_T$ mainly models fixed properties of the photodiode structure, as such is assumed to be constant for

TABLE I: Extracted parameters for the PIN10-D (100 mm$^2$)

| Bias (V) | $C_{pd}$ (nF) | $R_s$ ($\Omega$) | $R_T$ ($\Omega$) | $C_T$ (nF) | $L_s$ (nH) |
|---|---|---|---|---|---|
| 0 | 1.65 | 11.4 | 3.9 | 0.48 | 10 |
| 4 | 0.52 | 10.2 | 3.9 | 0.41 | 10 |
| 8 | 0.39 | 9.8 | 3.9 | 0.38 | 10 |
| 12 | 0.30 | 9.1 | 3.9 | 0.35 | 10 |

TABLE II: Extracted parameters for the PIN25-D (600 mm$^2$)

| Bias (V) | $C_{pd}$ (nF) | $R_s$ ($\Omega$) | $R_T$ ($\Omega$) | $C_T$ (nF) | $L_s$ (nH) |
|---|---|---|---|---|---|
| 0 | 9.6 | 2.8 | 1.9 | 0.2 | 17 |
| 4 | 3 | 2.7 | 1.9 | 0.18 | 17 |
| 8 | 2.2 | 2.6 | 1.9 | 0.17 | 17 |
| 12 | 1.8 | 2.5 | 1.9 | 0.16 | 17 |

each photodiode, irrespective of $V_B$.

As for the reactance of the photodiodes, it can be seen from Fig. 4 that for all $V_B$ cases, the two photodiodes exhibit a capacitive behaviour, as indicated by their negative Im($Z_{11}$) curves. Nevertheless, as the inductive effect of the feed-line dominates, the Im($Z_{11}$) becomes positive. The frequency at which Im($Z_{11}$) is zero corresponds to the LC resonance frequency, which is used to estimate both $C_{pd}$ and $L_s$. For the two photodiodes, increasing $V_B$ would increase $W_D$, which in turn reduces $C_{pd}$ as indicated by the reduction in the Im($Z_{11}$) curves (becomes more negative). Nevertheless, despite showing similar Im($Z_{11}$) trend, there is a notable difference in their respective values, by a factor of approximately 6 in all $V_B$ cases, as expected from the factor of 6 difference in their areas.

Hence, based on the photodiode parameter extraction above, it can be concluded that the photodiode equivalent circuit model of Fig. 1b gives a good estimation of the photodiode behaviour. In addition, the photodiode presents a sum of series resistances $R_s+R_T$ estimated to be in the range of 4 $\Omega$ to 15 $\Omega$ depending on the photodiode area and $V_B$. Although, such values appear small, they are relatively large compared to the input resistance of a low input impedance TIA stage such as the RGC, which can be as small as 1 $\Omega$ [6]. Therefore, in such a case, $R_s+R_T$ will impose an additional bandwidth-limiting effect on the VLC receiver. Moreover, the photodiodes demonstrated a capacitive behaviour at low frequencies corresponding to $C_{pd}$, which was dominated by the inductance of the feed-line at higher frequencies. The fitted parameter values of the photodiodes are presented in Tables I and II.

## IV. Low Input Impedance TIAs with Full Photodiode Modelling

This section highlights the importance of using the full equivalent circuit model of the photodiode, when designing the TIA, especially for low input impedance TIA configurations such as the RGC. This is accentuated through a design example of the RGC circuit, with the simplified photodiode equivalent model of Fig. 1a versus the full photodiode equivalent circuit model of Fig. 1b.

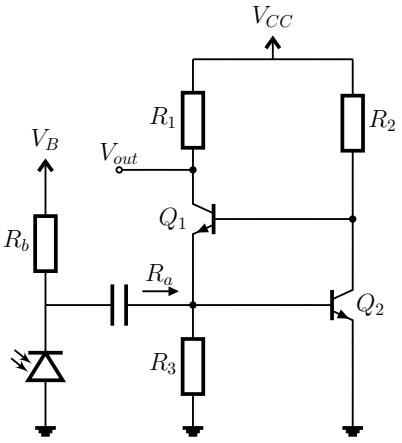


Fig. 5: RGC circuit with photodiode input

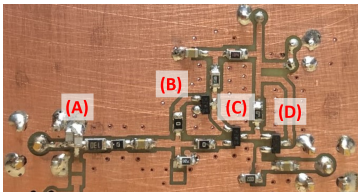


Fig. 6: RGC TIA PCB (A) Full photodiode equivalent model (B) CE ($Q_2$) stage (C) CB ($Q_1$) stage (D) Output buffer stage

### A. Low Input Impedance TIA design

Fig. 5 shows the RGC configuration, which is widely described as a modification to the common base (CB) stage ($Q_1$) with feedback presented by a common emitter (CE) stage ($Q_2$); this has the benefit of reducing the input resistance by a factor approximately equals the voltage gain of the CE. Hence, the RGC input resistance $R_a$ is given by:

$$R_a = \frac{1}{g_{m1}(1 + g_{m2}R_2)}) \tag{4}$$

where $g_{m1}$ and $g_{m2}$ are the transconductances of $Q_1$ and $Q_2$, respectively, and $R_2$ is the load resistor of $Q_2$. Such configuration features ultra-low input resistance in the range of a few Ohms to a fraction of an Ohm, which advantageously offers high tolerance to exceptionally high $C_{pd}$. Details on the operation and design of the RGC and a modified variant of the RGC TIA are studied in detail in [6].

Using discrete components, the RGC described above was built and test, with the addition of an output buffer (common collector (CC) stage). Fig. 6 shows the fabricated FR4 double-sided PCB of the RGC TIA. The PCB is populated using the NPN transistors BFU520A ($f_T$ = 10 GHz) and surface mount devices (SMD) for resistors and capacitors. The RGC is biased at collector currents of $Q_1$ and $Q_2$ is set to $I_{C1}$ = 1 mA, $I_{C2}$ = 4 mA, respectively. The transimpedance gain is set by $R_1$ = 1 k$\Omega$. Whereas, $R_2$ = 150 $\Omega$ at a supply voltage $V_{CC}$ = 9 V. The photodiode equivalent model are based on the PIN10-D extracted parameter values at $V_B$ = 12 V presented in Table I.

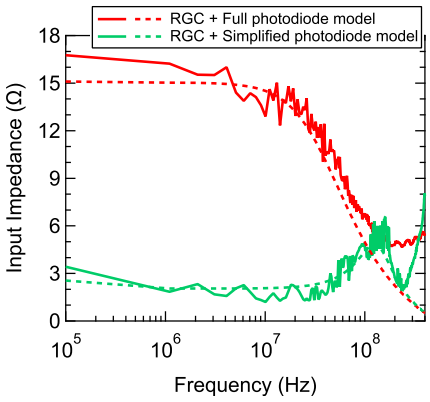


(a)

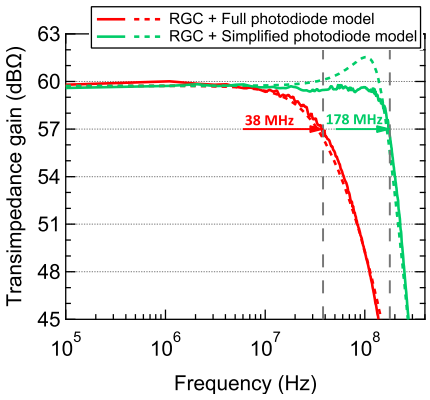


(b)

Fig. 7: Measured (solid) and simulated (dashed) RGC TIA responses with simplified photodiode model versus full photodiode model (a) Input impedance (b) Transimpedance gain

To test the performance of the TIA, first, the scattering parameters of the fabricated RGC TIA is measured using a VNA. These are then converted into the corresponding impedance parameters to obtain the input impedance and transimpedance gain responses. To facilitate the measurements, the photodiode is initially modelled as just a capacitor $C_{pd}$ equals 300 pF and then using the full photodiode equivalent model of Fig. 1b. The measured results are compared to the simulated results, where the simulated results are based on post PCB layout. The simulation considers the effect of a) PCB parasitic effects b) input transmission lines c) input capacitor models.

Fig. 7 shows the measured and simulated input impedance and transimpedance gain responses of the RGC TIA for the full photodiode equivalent circuit model versus the simplified one. From Fig. 7a, it can be clearly seen that the sum of resistances $R_s + R_T$ adds to the TIAs input resistance, which significantly enhances its value compared to the simplified model (resistance increase from approximately 1 Ω to 14 Ω). Consequently, the bandwidth of the TIA drops substantially, as illustrated by the corresponding transimpedance gain responses in Fig. 7b. As such, clearly using the simplified photodiode equivalent model results in overestimating the TIA bandwidth and may mislead the TIA design.

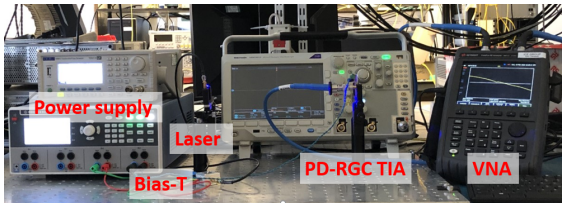


Fig. 8: Experimental set-up to test the optoelectronic response of the PIN10-D and the RGC TIA

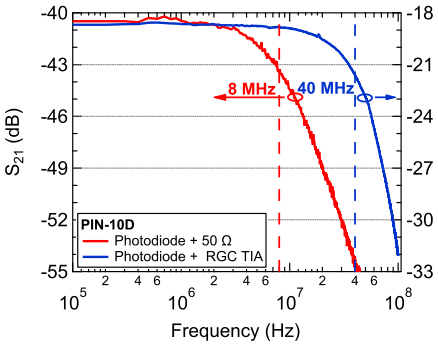


Fig. 9: Measured $S_{21}$ response of the optical link employing the PIN10-D (100 mm$^2$) and the RGC TIA versus the PIN10-D and a 50 Ω impedance

### B. Optical link Measurements

Fig. 8 shows the experimental set-up used to test the optoelectronic response of the PIN10-D with the RGC TIA. The set-up consists of a PL405 commercial blue laser diode transmitter, the large-area photodiode and the RGC TIA circuit built on PCB at the receiver. The laser diode is biased using a Mini-Circuit (ZFBT-4R2GWFT+) bias-T and is driven using port 1 of the VNA. A short free-space optical channel of a fixed distance connects the laser's output to the optical receiver assembly. The photodiode is reverse biased in the same manner as in Section III by grounding the anode and applying $V_B$ to the cathode through a bias resistor $R_b$ at $V_B = 12$ V. The cathode is AC-coupled to the RGC TIA, and port 2 of the VNA monitors the receiver's output. Noting that the bandwidth of the laser diode was verified to be approximately 2 GHz at $I_f = 35$ mA, which is well above the predicted bandwidths of the receiver assembly, including the large-area photodiode and the RGC TIA. Hence, the $S_{21}$ measurements of the overall link would accurately reflect the receiver performance only.

The optoelectrical response of the PIN10-D is measured independently and with the application of the RGC TIA. Fig. 9 shows the measured $S_{21}$ response of the PIN10-D (100 mm$^2$) when connected to the RGC TIA versus a 50 Ω. The figure indicates the gain of the RGC by having two y-axes. From Fig. 9, when connecting the photodiode to a 50 Ω, the bandwidth is largely determined by an RC time constant associated with the 50 Ω and the photodiode capacitance that approximates to 300 pF and hence, the cut-off-frequency is 8 MHz. On the other

hand, in the case of the RGC TIA, a substantial bandwidth enhancement compared to the 50 Ω, of approximately five-fold. This significant bandwidth enhancement results from the extremely low input resistance of the RGC TIA, which pushes the frequency of the dominant input pole to higher frequencies. Moreover, the measured $S_{21}$ bandwidth obtained matches the bandwidth predictions obtained by the simulations and measurements of the RGC TIA with the full photodiode passive equivalent circuit model. Whereas, the bandwidth obtained from the simplified passive equivalent model offered inaccurate predictions of the TIA bandwidth.

Hence, based on the findings of the design example of the RGC TIA initially using discrete components to emulate the simplified and full photodiode passive equivalent models and then the frequency response measurements of the optical link using the PIN10-D and the RGC TIA, it can be concluded that the model shown in Fig. 1b provides a reasonably accurate estimation of the photodiode behaviour. Moreover, extracting the photodiode model parameters prior to the design of the TIA is of importance in identifying the key bandwidth-limiting elements. Therefore, this procedure should be extended to the design of all optical receivers. This helps avoid inaccurate predictions of the receiver's bandwidth as encountered in [6], where the traditional approach of photodiode modelling was followed, and the effect of the photodiode intrinsic and extrinsic parasitic elements including $R_s$, $R_T$, $C_T$ and $L_p$ were ignored, leading to over-estimation of the receiver bandwidth. Omitting such elements, especially the photodiode series resistance, is a common pitfall for most circuit designers, therefore, care must be taken to account for such elements when designing TIA circuits for VLC applications.

## V. Conclusion

This work reports an equivalent circuit model of large-area PIN photodiodes for VLC applications. The model considers the photodiode intrinsic elements and other parasitic effects due to extrinsic factors. Model parameter extraction was conducted based on one-port impedance measurements of two commercially available large-area photodiodes. The model was shown to be highly accurate in fitting the impedance behaviour of the photodiodes. Furthermore, the model parameter established the presence of the photodiode series resistance, which was demonstrated to act as an additional bandwidth-limiting factor for VLC receivers, particularly when employing low input impedance TIAs. A design example of the low input impedance RGC TIA was described and constructed using discrete components on a PCB. The TIA was measured with the proposed photodiode equivalent circuit model and a simplified model to predict its bandwidth performance. In addition, a VLC link was constructed to measure the optoelectrical response ($S_{21}$) of the photodiode and the RGC TIA. This was contrasted to the measured bandwidth predictions, based on the photodiode equivalent circuit models, which verified that, unlike the simplified model, the proposed photodiode equivalent circuit model can accurately predict performance.

## References


[1] J. L. Cura and L. N. Alves, "Bandwidth improvements in transimpedance amplifiers for visible-light receiver front-ends," in *20th IEEE International Conference on Electronics, Circuits, and Systems (ICECS)*, 2013, pp. 831–834.

[2] R. Aguiar, A. Tavares *et al.*, "Considerations on the design of transceivers for wireless optical LANs," in *IEE Colloquium on Optical Wireless Communications*, 1999, pp. 2/1–231.

[3] B. Wilson and I. Darwazeh, "Low input resistance transimpedance optical preamplifier for fibre optic local area networks," in *1988., IEEE International Symposium on Circuits and Systems*, vol. vol.3, 1988, pp. 2531–2534.

[4] S. Giannakopoulos, Z. S. He *et al.*, "Differential common base TIA with 56 dB ohm gain and 45 GHz bandwidth in 130 nm SiGe," in *IEEE Asia Pacific Microwave Conference (APMC)*, 2017, pp. 1107–1110.

[5] S. M. Park and H.-J. Yoo, "1.25-Gb/s regulated cascode CMOS transimpedance amplifier for gigabit ethernet applications," *IEEE Journal of Solid-State Circuits*, vol. 39, no. 1, pp. 112–121, 2004.

[6] A. Kassem and I. Darwazeh, "Practical demonstration of RGC and modified RGC TIAs for VLC systems," in *28th IEEE International Conference on Electronics, Circuits, and Systems (ICECS)*, 2021.

[7] B. Huang and H. Chen, "A monolithic optical receiver chip for free space visible light communication system," in *11th IEEE International Conference on Solid-State and Integrated Circuit Technology*, 2012, pp. 1–3.

[8] E. S. Parapari, E. S. Parapari, and Z. D. Koozehkanani, "A broadband transimpedance amplifier (TIA) for visible light communication in 0.18-$\mu$m CMOS," in *2020 28th Iranian Conference on Electrical Engineering (ICEE)*, 2020, pp. 1–4.

[9] R. Y. Chen and Z.-Y. Yang, "CMOS transimpedance amplifier for visible light communications," *IEEE Transactions on Very Large Scale Integration (VLSI) Systems*, vol. 23, no. 11, 2015.

[10] S. Fuada, A. P. Putra *et al.*, "Trans-impedance amplifier design for visible light communication (VLC) using commercially available OP-AMP," in *2016 3rd International Conference on Information Technology, Computer, and Electrical Engineering (ICITACEE)*, 2016, pp. 31–36.

[11] L. Shi, L. K. Nanver *et al.*, "Series resistance optimization of high-sensitivity si-based VUV photodiodes," in *IEEE International Instrumentation and Measurement Technology Conference*, 2011, pp. 1–4.

[12] T. P. Lee, "Effect of junction capacitance on the rise time of LED's and on the turn-on delay of injection lasers," *The Bell System Technical Journal*, vol. 54, no. 1, pp. 53–68, 1975.

[13] W. Cheung, P. Edwards, and G. French, "Determination of LED equivalent circuits using network analyser measurements," in *Conference on Optoelectronic and Microelectronic Materials and Devices*, 1998, pp. 232–235.

[14] X. Li, Z. Ghassemlooy *et al.*, "An equivalent circuit model of a commercial LED with an ESD protection component for VLC," *IEEE Photonics Technology Letters*, vol. 33, no. 15, pp. 777–779, 2021.

[15] A. Kassem and I. Darwazeh, "Use of negative impedance converters for bandwidth extension of optical transmitters," *IEEE Open Journal of Circuits and Systems*, pp. 101–112, 2021.

[16] A. Steinbach, I. Penn *et al.*, "Equivalent circuit modelling of p-i-n photodiodes for 40 Gb/s receivers," in *15th Annual Meeting of the IEEE Lasers and Electro-Optics Society*, vol. 2, 2002, pp. 486–487.

[17] Z. Xu and J. Gao, "Semi-analytical small signal parameter extraction method for PIN photodiode," *IET Optoelectronics*, vol. 11, no. 3, pp. 103–107, 2017.

[18] O. Optoelectroncis, "Photodiode characteristics and applications," https://www.osioptoelectronics.com/application-notes/an-photodiode-parameters-characteristics.pdf, Accessed: 2022-03-02.

[19] L. Moura and I. Darwazeh, *Introduction to linear circuit analysis and modelling: from DC to RF*. Elsevier, 2005.